Eur. Phys. J. C 10, 51–62 (1999)
Digital Object Identifier (DOI) 10.1007/s100529900048

THE EUROPEAN PHYSICAL JOURNAL C

The rare K decays and Z^0 penguin contributions in the topcolor-assisted technicolor models

Zhenjun Xiao[1,2,3,a], Chongsheng Li[1,2], Kuangta Chao[1,2]

[1] CCAST (World Laboratory), P.O. Box 8730, Beijing 100080, P.R. China
[2] Department of Physics, Peking University, Beijing 100871, P.R. China
[3] Department of Physics, Henan Normal University, Xinxiang 453002, P.R. China

Received: 24 November 1998 / Revised version: 16 February 1999 / Published online: 15 July 1999

Abstract. We calculate the new contributions to the rare decays $K^+ \to \pi^+\nu\bar{\nu}$, $K_L \to \pi^0\nu\bar{\nu}$ and $K_L \to \mu^+\mu^-$ from new Z^0 penguin and box diagrams induced by the unit-charged scalars $(\tilde{\pi}^\pm, \tilde{H}^\pm, \pi_1^\pm, \pi_8^\pm)$ appearing in the topcolor-assisted technicolor (TC2) models. We find that: (a) the unit-charged top-pion $\tilde{\pi}^\pm$ and b-pion $\tilde{H}^\pm$ can provide large contributions to the rare K decays if they are relatively light; (b) the size of the mixing elements $D_{L,R}^{ij}$ $(i \neq j)$ is strongly constrained by the data of B^0 meson mixing: $|a_R^{ts}|, |a_R^{td}| < 0.01$ for $a_L^{td} = a_L^{ts} = 1/2$ and $m_{\tilde{H}^0} \leq 600\,\mathrm{GeV}$; (c) the enhancements to the branching ratios of rare K decays from new scalars can be as large as one order of magnitude; (d) there is a strong cancellation between the short- and the long-distance dispersive part of the decay $K_L \to \mu^+\mu^-$, the constraint on the new short-distance part from this decay mode is thus not strong; (e) the typical TC2 model under study is generally consistent with the available rare K-decay data.

1 Introduction

As is well known, the study of loop effects can open an important window on electroweak symmetry breaking and physics beyond the standard model (SM). The examination of indirect effects of new physics in flavor changing neutral current (FCNC) processes in rare K and B decays [1–5] offers a complementary approach to the search for the direct production of new particles at high energy colliders.

In the SM, the rare K decays $K^+ \to \pi^+\nu\bar{\nu}$, $K_L \to \pi^0\nu\bar{\nu}$ and $K_L \to \mu^+\mu^-$ are all loop-induced semileptonic FCNC processes determined by Z^0 penguin and W box diagrams [1]. Since these rare decay modes are theoretically clean and highly suppressed in the SM, they may serve as a good hunting ground for new physics beyond the SM. Furthermore, relevant experimental measurements now reach a reasonable or even high sensitivity [6,7], which will help us to test or constrain the new physics models through studies of these rare decay modes.

In [2,3], the authors studied the FCNC effects on the mixing and rare decays for the K and B meson systems in the minimal supersymmetric standard model and the two Higgs doublet model. In this paper we will investigate the new contributions to the rare K decays from the Z^0 penguin diagrams induced by the unit-charged scalars appearing in the TC2 model [8].

[a] e-mail: zxiao@ibm320h.phy.pku.edu.cn and dphnu@public.zz.ha.cn.

Technicolor (TC) [9,10] is one of the important candidates for the mechanism of naturally breaking electroweak symmetry. To generate ordinary fermion masses, extended technicolor (ETC) [11] models have been proposed. In walking technicolor theories [12], the large FCNC problem can be resolved and the fermion masses can be increased significantly [12]. The S parameter can be small or even negative in the walking technicolor models [13]. To explain the large hierarchy of the quark masses, multiscale walking technicolor models (MWTCM) are further constructed [14]. In order to generate a large top-quark mass without running afoul of either experimental constraints from the ρ parameter and the R_b data, TC2 models were constructed recently [8,15,16].

In the TC2 model, the relatively light top-pions $(\tilde{\pi}^\pm, \tilde{\pi}^0)$, b-pions $(\tilde{H}^\pm, \tilde{H}^0, \tilde{A}^0)$ and other bound states may provide potentially large loop effects in low energy observables. This is the main motivation for us to investigate the contributions to the rare K decays from the penguin and box diagrams induced by the internal exchanges of unit-charged top-pions, b-pions and technipions.

In a previous paper [4], we calculated the Z^0 penguin contributions to the rare K decays from technipions $\pi_1^\pm$ and $\pi_8^\pm$ in the MWTCM [14] and found that this model was strongly disfavored by the relevant data.

In this paper we calculate the new Z^0 penguin contributions to the rare K decays from the top-pions $\tilde{\pi}^\pm$, b-pions $\tilde{H}^\pm$ and technipions $\pi_1^\pm$ and $\pi_8^\pm$ appearing in the TC2 model [8]. We firstly evaluate the Z^0 penguin and box

diagrams induced by the unit-charged scalars, compare the relevant analytical expressions of effective couplings with the corresponding expressions in the SM, separate the new functions $C_0(\pi_i)$ and $C_{\rm NL}\pi_i$ ($\pi_i = \tilde{\pi}^{\pm}, \tilde{\rm H}^{\pm}, \pi_1^{\pm}, \pi_8^{\pm}$) which describe the effects of the new particles, and finally combine the new functions with their counterparts in the SM and use them directly in the calculation for specific decay modes.

This paper is organized as follows. In Sect. 2 we briefly review the basic structures of the TC2 models and study the experimental constraints on the mixing matrices $D_{\rm L}$ and $D_{\rm R}$. In Sect. 3 we firstly show the standard-model predictions for the branching ratios of rare K decays, and then evaluate the new one-loop Feynman diagrams and extract out the new effective Z^0 penguin couplings induced by the exchanges of unit-charged scalars. In following two sections, we present the numerical results for the branching ratios $B(K^+ \to \pi^+\nu\bar{\nu})$, $B(K_L \to \pi^0\nu\bar{\nu})$ and $B(K_L \to \mu^+\mu^-)_{\rm SD}$ with the inclusion of new physics effects and compare the theoretical predictions with the available data. The conclusions and discussions are included in the final section.

2 Basic structure of TC2 models

Apart from some differences in group structure and/or particle contents, all TC2 models [8,15,16] have the following common features: (a) strong topcolor interactions, broken near 1 TeV, induce a large top condensate and all but a few GeV of the top-quark mass, but contribute little to electroweak symmetry breaking; (b) TC interactions are responsible for electroweak symmetry breaking, and ETC interactions generate the hard masses of all quarks and leptons, except that of the top quarks; (c) there exist top-pions $\tilde{\pi}^{\pm}$ and $\tilde{\pi}^0$ with a decay constant $f_{\tilde{\pi}} \approx 50\,{\rm GeV}$. In this paper we will chose the most frequently studied TC2-I model [8][1] as the typical TC2 model to estimate the contributions to the rare K decays in question from the relatively light unit-charged scalars. It is straightforward to extend the studies in this paper to other TC2 models.

2.1 TC2-I model, couplings and mass spectrum

In the TC2-I model [8] the dynamics at the scale ∼1 TeV involves the following structure:

$$\begin{aligned} &{\rm SU(3)_1 \times U(1)_{Y1} \times SU(3)_2 \times U(1)_{Y2} \times SU(2)_L} \\ &\quad \to {\rm SU(3)_{QCD} \times U(1)_{EM}}, \end{aligned} \tag{1}$$

where $\mathrm{SU(3)_1 \times U(1)_{Y1}}$ ($\mathrm{SU(3)_2 \times U(1)_{Y2}}$) generally couples preferentially to the third (first and second) generation fermions. The breaking (1) typically leaves a residual global symmetry, $\mathrm{SU(3)' \times U(1)'}$, implying a degenerate, massive color-octet of coloron (i.e. the top-gluon) V_μ^α ($\alpha = 1, 2, \cdots, 8$) and a color-singlet heavy Z'_μ. The gluon A_μ^α and coloron V_μ^α (the SM $\mathrm{U(1)_Y}$ field B_μ and the $\mathrm{U(1)'}$ field Z'_μ) are then defined by orthogonal rotations with mixing angle θ (θ'):

$$\begin{aligned} h_1 \sin\theta = h_2 \cos\theta = g_3, \quad \cot\theta = \frac{h_1}{h_2}, \\ q_1 \sin\theta' = q_2 \cos\theta' = g_1, \quad \cot\theta' = \frac{q_1}{q_2}, \end{aligned} \tag{2}$$

where h_1, h_2, q_1, and q_2 are coupling constants of $\mathrm{SU(3)_1}$, $\mathrm{SU(3)_2}$, $\mathrm{U(1)_{Y1}}$ and $U()_{Y2}$, respectively, and g_3 (g_1) is the $\mathrm{SU(3)_C}$ ($\mathrm{U(1)_Y}$) coupling constant at $\Lambda_{\rm TC}$. In order to select the correct top-quark direction for condensation, one usually demands $\cot\theta >> 1$ and $\cot\theta' >> 1$.

Both the coloron V and the Z′ must be heavier than 1 TeV according to the experimental data from the Fermilab Tevatron [17,18]. After integrating out the heavy coloron and Z′, the effective four-fermion interactions have the form [19,20]

$$\begin{aligned} \mathcal{L}_{\rm eff} = \frac{4\pi}{M_{\rm B}^2} \Bigg\{ &\left(\kappa + \frac{2\kappa_1}{27}\right) \overline{\psi}_{\rm L} {\rm t_R} \bar{\rm t}_{\rm R} \psi_{\rm L} \\ &+ \left(\kappa - \frac{\kappa_1}{27}\right) \overline{\psi}_{\rm L} {\rm b_R} \bar{\rm b}_{\rm R} \psi_{\rm L} \Bigg\}, \end{aligned} \tag{3}$$

where $\kappa = (g_3^2/4\pi)\cot^2\theta$ and $\kappa_1 = (g_1^2/4\pi)\cot^2\theta'$, and $M_{\rm B}$ is the mass of coloron V^α and Z′.

The effective interactions of (3) can be written in terms of two auxiliary scalar doublets ϕ_1 and ϕ_2. Their couplings to quarks are given by [21]

$$\mathcal{L}_{\rm eff} = \lambda_1 \overline{\psi}_{\rm L} \phi_1 \bar{\rm t}_{\rm R} + \lambda_2 \overline{\psi}_{\rm L} \phi_2 \bar{\rm b}_{\rm R}, \tag{4}$$

where $\lambda_1^2 = 4\pi(\kappa + 2\kappa_1/27)$ and $\lambda_2^2 = 4\pi(\kappa - \kappa_1/27)$. At energies below the topcolor scale $\Lambda \sim 1\,{\rm TeV}$, the auxiliary fields acquire kinetic terms, becoming physical degrees of freedom. The properly renormalized ϕ_1 and ϕ_2 doublets take the form

$$\phi_1 = \begin{pmatrix} f_{\tilde{\pi}} + \frac{1}{\sqrt{2}}({\rm h_t} + {\rm i}\tilde{\pi}^0) \\ \tilde{\pi}^- \end{pmatrix} \tag{5}$$

and

$$\phi_2 = \begin{pmatrix} \tilde{\rm H}^+ \\ \frac{1}{\sqrt{2}}(\tilde{\rm H}^0 + {\rm i}\tilde{\rm A}^0) \end{pmatrix}, \tag{6}$$

where $\tilde{\pi}^{\pm}$ and $\tilde{\pi}^0$ are the top-pions, $\tilde{\rm H}^{\pm,0}$ and $\tilde{\rm A}^0$ are the b-pions, $\rm h_t$ is the top-Higgs [20], and $f_{\tilde{\pi}} \approx 50\,{\rm GeV}$ is the top-pion decay constant.

From (4), the couplings of top-pions to the t- and b-quark can be written as [8]:

$$\frac{m_{\rm t}^*}{f_{\tilde{\pi}}} \left[{\rm i}\bar{\rm t}{\rm t}\tilde{\pi}^0 + {\rm i}\bar{\rm t}_{\rm R}{\rm b}_{\rm L}\tilde{\pi}^+ + \frac{m_{\rm b}^*}{m_{\rm t}^*}\bar{\rm t}_{\rm L}{\rm b}_{\rm R}\tilde{\pi}^+ + {\rm h.c.} \right]. \tag{7}$$

Here, $m_{\rm t}^* = (1-\epsilon)m_{\rm t}$ and $m_{\rm b}^* \approx 1\,{\rm GeV}$ denote the masses of the top and bottom quarks generated by topcolor interactions.

[1] In this paper, we use the term "TC2-I" model to denote the TC2 model constructed by Hill [8].

For the mass of top-pions, the current $1-\sigma$ lower mass bound from the Tevatron data is $m_{\tilde{\pi}} \geq 150\,\mathrm{GeV}$ [15], while the theoretical expectation is $m_{\tilde{\pi}} \approx (150 - 300\,\mathrm{GeV})$ [8]. For the mass of the b-pions, the current theoretical estimation is $m_{\tilde{\mathrm{H}}^0} \approx m_{\tilde{\mathrm{A}}^0} \approx (100\text{–}350)\,\mathrm{GeV}$ and $m_{\tilde{\mathrm{H}}} = m^2_{\tilde{\mathrm{H}}^0} + 2m^2_{\mathrm{t}}$ [17]. For the color-singlet $\pi_1^{\pm}$ and color-octet $\pi_8^{\pm}$, the current theoretical estimations are $m_{\pi_1} \geq 50\,\mathrm{GeV}$ and $m_{\pi_8} \approx 200\,\mathrm{GeV}$ [22,4]. In this paper we conservatively consider a little wider mass ranges of new scalars:

$$\begin{aligned} m_{\tilde{\pi}} &= (100 \sim 500)\,\mathrm{GeV}, \quad m_{\tilde{\mathrm{H}}} = (300\text{–}1000)\,\mathrm{GeV}, \\ m_{\tilde{\mathrm{H}}^0,\tilde{\mathrm{A}}^0} &= (150\text{–}600)\,\mathrm{GeV}, \quad m_{\pi_1} = (50\text{–}100)\,\mathrm{GeV}, \\ m_{\pi_8} &= (100\text{–}300)\,\mathrm{GeV}. \end{aligned} \tag{8}$$

For $f_{\tilde{\pi}}$ and ϵ, we use $f_{\tilde{\pi}} = (50\text{–}60)\,\mathrm{GeV}$ and $\epsilon = (0.03\text{–}0.1)$ [8,21].

The effective Yukawa couplings of ordinary technipions $\pi_1^{\pm}$ and $\pi_8^{\pm}$ to fermion pairs can be found in [4,22,23]. The relevant gauge couplings of unit-charged scalars to the Z^0 gauge boson are basically model-independent and can be written as [4,22]

$$Z\pi_i^+\pi_i^- : \ -\mathrm{i}g\frac{1-2\sin^2\theta_{\mathrm{W}}}{2\cos\theta_{\mathrm{W}}}(p^+ - p^-)\cdot\epsilon', \tag{9}$$

$$Z\pi_{8\alpha}^+\pi_{8\beta}^- : \ -\mathrm{i}g\frac{1-2\sin^2\theta_{\mathrm{W}}}{2\cos\theta_{\mathrm{W}}}(p^+ - p^-)\delta_{\alpha\beta}\cdot\epsilon', \tag{10}$$

where θ_{W} is the Weinberg angle, p^+ and p^- are the momenta of relevant scalars, ϵ' is the polarization vector of the Z^0 gauge boson, and π_i denotes the color-singlet scalars $\tilde{\pi}^{\pm}$, $\tilde{\mathrm{H}}^{\pm}$ and $\pi_1^{\pm}$, respectively.

2.2 The square-root ansatz and experimental constraints

At low energy, potentially large FCNCs arise when the quark fields are rotated from their weak eigenbasis to their mass eigenbasis, realized by the matrices $U_{\mathrm{L,R}}$ for the up-type quarks, and by $D_{\mathrm{L,R}}$ for the down-type quarks. When we make the replacements, for example,

$$\mathrm{b_L} \to D_{\mathrm{L}}^{\mathrm{bd}}\mathrm{d_L} + D_{\mathrm{L}}^{\mathrm{bs}}\mathrm{s_L} + D_{\mathrm{L}}^{\mathrm{bb}}\mathrm{b_L}, \tag{11}$$

$$\mathrm{b_R} \to D_{\mathrm{R}}^{\mathrm{bd}}\mathrm{d_R} + D_{\mathrm{R}}^{\mathrm{bs}}\mathrm{s_R} + D_{\mathrm{R}}^{\mathrm{bb}}\mathrm{b_R}, \tag{12}$$

the FCNC interactions will be induced. In the TC2-I model, the corresponding flavor changing effective Yukawa couplings are

$$\begin{aligned} &\frac{m_{\mathrm{t}}^*}{f_{\tilde{\pi}}}\left[\mathrm{i}\tilde{\pi}^+(D_{\mathrm{L}}^{\mathrm{bs}}\bar{\mathrm{t}}_{\mathrm{R}}\mathrm{s_L} + D_{\mathrm{L}}^{\mathrm{bd}}\bar{\mathrm{t}}_{\mathrm{R}}\mathrm{d_L})\right. \\ &\left.\quad +\mathrm{i}\tilde{\mathrm{H}}^+(D_{\mathrm{R}}^{\mathrm{bs}}\bar{\mathrm{t}}_{\mathrm{L}}\mathrm{s_R} + D_{\mathrm{R}}^{\mathrm{bd}}\bar{\mathrm{t}}_{\mathrm{L}}\mathrm{d_R}) + \mathrm{h.c.}\right]. \end{aligned} \tag{13}$$

Although there are many discussions about the mixing matrices in the TC2 models [8,19,21,24], there exist no "standard" mixing matrixes currently. In the literature, authors usually use the "square-root ansatz": to take the square root of the standard-model CKM matrix ($V_{\mathrm{CKM}} = U_{\mathrm{L}}^+ D_{\mathrm{L}}$) as an indication of the size of realistic mixings. It should be denoted that the square-root ansatz must be modified because of the strong constraints from the data of B^0–$\overline{\mathrm{B}^0}$ mixing [21,24].

In the SM, the B^0 meson mixings occur in second-order weak interactions. There is evidence for B^0–$\overline{\mathrm{B}^0}$ mixing with $\Delta M_{\mathrm{B_d}} = (3.05 \pm 0.12) \times 10^{-10}\,\mathrm{MeV}$ [25], and for $\mathrm{B_s^0}$–$\overline{\mathrm{B_s^0}}$ mixing, with $\Delta M_{\mathrm{B_s}} > 6 \times 10^{-9}\,\mathrm{MeV}$ (CL = 95%) [25].

In TC2 models, the neutral scalars $\tilde{\mathrm{H}}^0$ and $\tilde{\mathrm{A}}^0$ can induce a contribution to the B_q^0–$\overline{\mathrm{B}}_q^0$ ($q = \mathrm{d}, \mathrm{s}$) mass difference [19,21]

$$\frac{\Delta M_{\mathrm{B}_q}}{M_{\mathrm{B}_q}} = \frac{7}{12}\frac{m_{\mathrm{t}}^2}{f_{\tilde{\pi}}^2 m_{\tilde{\mathrm{H}}^0}^2}\delta_{\mathrm{b}q}B_{\mathrm{B}_q}F_{\mathrm{B}_q}^2, \tag{14}$$

where M_{B_q} is the mass of the B_q meson, F_{B_q} is the B_q meson decay constant, B_{B_q} is the renormalization group invariant parameter, and $\delta_{\mathrm{b}q} \approx |D_{\mathrm{L}}^{\mathrm{b}q} D_{\mathrm{R}}^{\mathrm{b}q}|$. For the $\mathrm{B_d}$ meson, using the data of $\Delta M_{\mathrm{B_d}} = (3.05 \pm 0.12) \times 10^{-10}\,\mathrm{MeV}$ [25] and setting $f_{\tilde{\pi}} = 50\,\mathrm{GeV}$, $\sqrt{B_{\mathrm{B_d}}}F_{\mathrm{B_d}} = 200\,\mathrm{MeV}$ [1], one has the bound

$$\delta_{\mathrm{b}d} \leq 0.76 \times 10^{-7} \tag{15}$$

for $m_{\tilde{\mathrm{H}}^0} \leq 600\,\mathrm{GeV}$. This is an important and strong bound on the product of mixing elements $D_{\mathrm{L,R}}^{\mathrm{bd}}$. As pointed in [19], if one naively uses the square-root ansatz for *both* D_{L} and D_{R}, the bound (15) is violated by about 2 orders of magnitude. As shown in [19], the "triangular texture" of the mixing matrix may provide a natural suppression of the effect by producing approximately diagonal D_{L} *or* D_{R} matrices. This will give $\delta_{\mathrm{bd}} \approx 0$ and avoids the bound.

Numerically, if we use the square-root ansatz for D_{L} itself and assume that $D_{\mathrm{L,R}}^{\mathrm{bd}}/V_{\mathrm{td}} = a_{\mathrm{L,R}}^{\mathrm{td}}$, then the bound (15) can be written in a new form:

$$|a_{\mathrm{R}}^{\mathrm{td}}| \leq 1.7 \times 10^{-3}, \tag{16}$$

for $a_{\mathrm{L}}^{\mathrm{td}} = 0.5$ and $m_{\tilde{\mathrm{H}}^0} \leq 600\,\mathrm{GeV}$. It is obviously a very strong constraint on $D_{\mathrm{R}}^{\mathrm{bd}}$.

For the $\mathrm{B_s}$ meson, the available data is only a lower bound on $\Delta m_{\mathrm{B_s}}$ [25]:

$$\Delta M_{\mathrm{B_s}} > 6 \times 10^{-9}\,\mathrm{MeV} = 19.6\Delta M_{\mathrm{B_d}}. \tag{17}$$

But one can get a reliable estimation of $\Delta M_{\mathrm{B_s}}$ from its relation with $\Delta M_{\mathrm{B_d}}$. In the ratio of $\mathrm{B_s}$ and $\mathrm{B_d}$ mass differences, many common factors cancel, and we have [25]

$$\begin{aligned} \Delta M_{\mathrm{B_s}} &= \Delta M_{\mathrm{B_d}}\frac{M_{\mathrm{B_s}}}{M_{\mathrm{B_d}}}\frac{B_{\mathrm{B_s}}F_{\mathrm{B_s}}^2}{B_{\mathrm{B_d}}F_{\mathrm{B_d}}^2}\frac{|V_{\mathrm{tb}}^* \cdot V_{\mathrm{ts}}|^2}{|V_{\mathrm{tb}}^* \cdot V_{\mathrm{td}}|^2} \\ &= 24.9\Delta M_{\mathrm{B_d}}, \end{aligned} \tag{18}$$

where we have used $M_{\mathrm{B_d}} = 5.279\,\mathrm{GeV}$, $M_{\mathrm{B_s}} = 5.369\,\mathrm{GeV}$, and $B_{\mathrm{B_s}}/B_{\mathrm{B_d}} = 1.01 \pm 0.04$ and $F_{\mathrm{B_s}}/F_{\mathrm{B_d}} = 1.15 \pm 0.05$ from lattice QCD [26]. Using (14) and (18), and assuming $D_{\mathrm{L,R}}^{\mathrm{bs}}/V_{\mathrm{ts}} = a_{\mathrm{L,R}}^{\mathrm{ts}}$, we have

$$|a_{\mathrm{R}}^{\mathrm{ts}}| \leq 1.6 \times 10^{-3}, \tag{19}$$

for $a_{\rm L}^{\rm ts}=0.5$ and $m_{\tilde{\rm H}^0}\leq 600\,{\rm GeV}$. From (17) and (18) we believe that the true value of $\Delta M_{\rm B_s}$ should be within the range of (19.6–24.9)$\Delta M_{\rm B_d}$. The inclusion of uncertainties of the data and input parameters will weaken the above constraints, but cannot change them greatly. It is thus reasonable to expect that both $|a_{\rm R}^{\rm td}|$ and $|a_{\rm R}^{\rm ts}|$ cannot be larger than 0.01 for $a_{\rm L}^{tj}\approx 1/2$ ($j={\rm d,s}$) and $m_{\tilde{\rm H}^0}\leq 600\,{\rm GeV}$. We conservatively use 0.01 as the upper bound on both $a_{\rm R}^{\rm ts}$ and $a_{\rm R}^{\rm td}$ afterwards.

In this paper we assume that all elements of $D_{\rm L}$ and $D_{\rm R}$ are real because we do not study CP violation here. We will consider the following two typical cases in the numerical calculation:

- Case A: We assume that $\epsilon=0.05$ and $f_{\tilde{\pi}}=50\,{\rm GeV}$, and we use the square-root ansatz for $D_{\rm L}$: $a_{\rm L}^{\rm ts}=a_{\rm L}^{\rm td}=1/2$, but we set $a_{\rm R}^{\rm ts}=a_{\rm R}^{\rm td}=0.01$.
- Case B: We assume that $\epsilon=0.05$ and $f_{\tilde{\pi}}=50\,{\rm GeV}$, and we use the square-root ansatz for *both* $D_{\rm L}$ and $D_{\rm R}$: $a_{\rm L}^{tj}=1/2, |a_{\rm R}^{tj}|=1/2$ (j= d, s).

Case A is consistent with the constraints from the data of $\rm B_q^0$–$\overline{\rm B_q^0}$ ($q={\rm d,s}$) mixing. For Case B, it violates the constraints (16) and (19). We still consider Case B here in order to see what will happen if we use the popular square-root ansatz for both $D_{\rm L}$ and $D_{\rm R}$.

In this paper, we fix the following relevant parameters [1,25] and use them as the standard input (SIP):

$$\begin{aligned} M_{\rm W}&=80.41\,{\rm GeV};\quad \alpha_{\rm em}=1/129;\\ \sin^2\theta_{\rm W}&=0.23;\quad m_{\rm c}\equiv\overline{m_{\rm c}}\\ (m_{\rm c})&=1.35\,{\rm GeV},\quad m_{\rm t}\equiv\overline{m_{\rm t}}\quad (m_{\rm t})=170\,{\rm GeV},\\ \mu_{\rm c}&=1.3\,{\rm GeV},\quad \mu_{\rm t}=170\,{\rm GeV},\\ \Lambda_{\overline{\rm MS}}^{(4)}&=0.325\,{\rm GeV},\quad \Lambda_{\overline{\rm MS}}^{(5)}=0.225\,{\rm GeV},\\ A&=0.84,\quad \lambda=0.22,\quad \rho=0,\quad \eta=0.36, \end{aligned}\tag{20}$$

where the A,λ,ρ and η are Wolfenstein parameters at the leading order. For $\alpha_{\rm s}(\mu)$ we use the two-loop expression as given in the second paper of [1].

3 Rare K decays and new physics effects

In this paper we use the "penguin box expansion" (PBE) approach [27]. One important advantage of this PBE approach is that the rare K decays in question depend only on one or two basic, universal, process-independent functions. At next-to-leading order (NLO), such functions are $X(x_{\rm t})$ and $X_{\rm NL}^l$ for decays $\rm K^+\to\pi^+\nu\overline{\nu}$ and $\rm K_L\to\pi^0\nu\overline{\nu}$, and $Y(x_{\rm t})$ and $Y_{\rm NL}$ for the short-distance part of the decay $\rm K_L\to\mu^+\mu^-$. The functions $X(x_{\rm t})$ and $Y(x_{\rm t})$ describe the dominant $m_{\rm t}$-dependent contributions, while the functions $X_{\rm NL}^l$ and $Y_{\rm NL}$ describe the $m_{\rm t}$-independent contributions stemming from internal quarks other than the top quark (usually known as the charm part).

3.1 Rare K decays in the SM

In the SM, the rare K decays $\rm K^+\to\pi^+\nu\overline{\nu}$, $\rm K_L\to\pi^0\nu\overline{\nu}$ and the short-distance part of $\rm K_L\to\mu^+\mu^-$ have been studied in great detail and were summarized for instance in a new review paper [1]. At the leading order (LO), the contributions to the rare K decays from $\rm Z^0$ penguin and W box diagrams are controlled by the functions $C_0(x_i)$ and $B_0(x_i)$ ($i={\rm u,c,t}$), which were evaluated long time ago by Inami and Lim [28]. In recent years, the NLO corrections have been calculated systematically by many authors [1]. The great progress in both the theoretical and experimental investigations enable us now to study the new physics effects on the rare K decays.

At the NLO level, the effective Hamiltonian for $\rm K^+\to\pi^+\nu\overline{\nu}$, $\rm K_L\to\pi^0\nu\overline{\nu}$ and $(\rm K_L\to\mu^+\mu^-)_{SD}$ can be written as [1]

$$\begin{aligned}\mathcal{H}_{\rm eff}(\rm K^+\to\pi^+\nu\overline{\nu})&=\frac{\alpha_{\rm em}G_{\rm F}}{2\sqrt{2}\pi\sin^2\theta_{\rm W}}\\ &\times\sum_{l={\rm e},\mu,\tau}\left[\lambda_{\rm t}X(x_{\rm t})+\lambda_{\rm c}X_{\rm NL}^l\right](\bar{\rm s}{\rm d})_{V-A}(\overline{\nu_l}\nu_l)_{V-A},\end{aligned}\tag{21}$$

$$\begin{aligned}\mathcal{H}_{\rm eff}(\rm K_L\to\pi^0\nu\overline{\nu})&=\frac{\alpha_{\rm em}G_{\rm F}}{2\sqrt{2}\pi\sin^2\theta_{\rm W}}\\ &\times\lambda_{\rm t}X(x_{\rm t})(\bar{\rm s}{\rm d})_{V-A}(\bar{\nu}\nu)_{V-A}+{\rm h.c.},\end{aligned}\tag{22}$$

$$\begin{aligned}\mathcal{H}_{\rm eff}((\rm K_L\to\mu^+\mu^-)_{SD})&=-\frac{\alpha_{\rm em}G_{\rm F}}{2\sqrt{2}\pi\sin^2\theta_{\rm W}}\\ &\times\left[\lambda_{\rm t}Y(x_{\rm t})+\lambda_{\rm c}Y_{\rm NL}\right](\bar{\rm s}{\rm d})_{V-A}(\overline{\mu}\mu)_{V-A}+{\rm h.c.},\end{aligned}\tag{23}$$

where $\alpha_{\rm em}$ is the electromagnetic fine-structure constant, $G_{\rm F}=1.16639\times10^{-5}\,{\rm GeV}^{-2}$ is the Fermi coupling constant, and $\lambda_i=V_{is}^*V_{id}$ and V_{ij} ($i={\rm u,c,t}; j={\rm d,s,b}$) are the elements of the CKM mixing matrix in the SM. The functions $X(x_{\rm t})$, $Y(x_{\rm t})$, $X_{\rm NL}^l$ and $Y_{\rm NL}$ are

$$X(x_{\rm t})=C_0(x_{\rm t})-4B_0(x_{\rm t})+\frac{\alpha_{\rm s}}{4\pi}X_1(x_{\rm t}),\tag{24}$$

$$Y(x_{\rm t})=C_0(x_{\rm t})-B_0(x_{\rm t})+\frac{\alpha_{\rm s}}{4\pi}Y_1(x_{\rm t}),\tag{25}$$

$$X_{\rm NL}^l=C_{\rm NL}-4B_{\rm NL}^{1/2},\tag{26}$$

$$Y_{\rm NL}=C_{\rm NL}-B_{\rm NL}^{-1/2},\tag{27}$$

where the functions $C_0(x_{\rm t})$ and $B_0(x_{\rm t})$ are leading top-quark contributions through the $\rm Z^0$ penguin and W box diagrams, respectively, $X_1(x_{\rm t})$ and $Y_1(x_{\rm t})$ are NLO QCD corrections, $C_{\rm NL}$ is the $\rm Z^0$ penguin part in the charm sector, and finally the functions $B_{\rm NL}^{1/2}$ and $B_{\rm NL}^{-1/2}$ are the W box contributions in the charm sector, relevant for the case of final state neutrinos (leptons) with weak isospin $T_3=1/2$ ($-1/2$), respectively.

Using the effective Hamiltonians (21) and (22), and summing over the three neutrino flavors we arrive at [1]

$$\begin{aligned}B(\rm K^+\to\pi^+\nu\overline{\nu})=\kappa_+\cdot\Bigg[&\left(\frac{{\rm Im}\lambda_{\rm t}}{\lambda^5}X(x_{\rm t})\right)^2+\left(\frac{{\rm Re}\lambda_{\rm c}}{\lambda}P_0(X)\right.\\ &\left.+\frac{{\rm Re}\lambda_{\rm t}}{\lambda^5}X(x_{\rm t})\right)^2\Bigg],\end{aligned}\tag{28}$$

$$B(\rm K_L\to\pi^0\nu\overline{\nu})=\kappa_{\rm L}\cdot\left(\frac{{\rm Im}\lambda_{\rm t}}{\lambda^5}X(x_{\rm t})\right)^2,\tag{29}$$

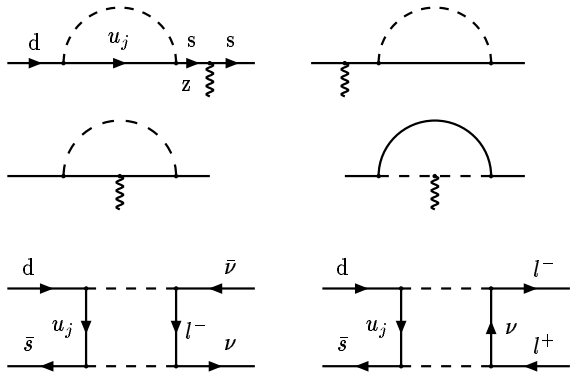

Fig. 1. The new Z^0 penguin and box diagrams induced by the internal exchanges of the unit-charged scalars $\pi_1^\pm$, $\pi_8^\pm$, $\tilde{\pi}^\pm$ and $\tilde{H}^\pm$. The dashed lines are scalars and the u_j stands for the up-type quarks (u, c, t)

where $\kappa_+ = 4.11 \times 10^{-11}$ and $\kappa_L = 1.80 \times 10^{-10}$ as given in [1].

For the short-distance part of $K_L \to \mu^+\mu^-$, we have

$$B(K_L \to \mu^+\mu^-)_{SD} = \kappa_\mu \cdot \left[\frac{\mathrm{Re}\lambda_c}{\lambda} P_0(Y) + \frac{\mathrm{Re}\lambda_t}{\lambda^5} Y(x_t)\right]^2, \quad (30)$$

where $\kappa_\mu = 1.68 \times 10^{-9}$ [1]. The functions $P_0(X)$ and $P_0(Y)$ in (28) and (30) describe the contributions from the charm sector and have been defined in [1]:

$$P_0(X) = \frac{1}{\lambda^4}\left[\frac{2}{3}X_{NL}^e + \frac{1}{3}X_{NL}^\tau\right] \quad (31)$$

$$P_0(Y) = \frac{Y_{NL}}{\lambda^4}. \quad (32)$$

The explicit expressions for the functions $C_0(x_t)$, $B_0(x_t)$, $X_1(x_t)$, $Y_1(x_t)$, C_{NL}, $B_{NL}^{1/2}$ and $B_{NL}^{-1/2}$ can be found for instance in [1]. For the convenience of the reader, we present these functions in Appendix A.

3.2 New Z^0 penguin contributions in the TC2-I model

For the rare K decays under consideration, the new physics will manifest itself by modifying the functions $X(x_t)$ and $Y(x_t)$, as well as the functions X_{NL} and Y_{NL} in effective Hamiltonians (21), (22), and (23).

The new one-loop diagrams can be obtained from the diagrams in the SM by replacing the internal $W^\pm$ lines with the unit-charged scalar lines, as shown in Fig. 1. The color-octet $\pi_8^\pm$ does not couple to the $l\nu$ lepton pairs, and therefore is not present in the box diagrams. Regarding the color-singlet scalars, they do couple to $l\nu$ pairs through box diagrams, but the relevant couplings are strongly suppressed by the lightness of m_l. Consequently, we can safely neglect the tiny contributions from those scalars through the box diagrams.

In [4], we evaluated the new one-loop Z^0 penguin and W box diagrams for the induced $d\bar{s}Z$ couplings due to the exchange of unit-charged technipions $\pi_1^\pm$ and $\pi_8^\pm$ in the multiscale walking technicolor model [14]. In this paper we use the same method and follow the same procedure to evaluate the one-loop diagrams induced by top-pions $\tilde{\pi}^\pm$ and b-pions $\tilde{H}^\pm$.

We will use dimensional regularization to regulate all the ultraviolet divergences in the virtual loop corrections and adopt the $\overline{MS}$ renormalization scheme. It is easy to show that all ultraviolet divergences are canceled for scalars $\tilde{\pi}^\pm$, $\tilde{H}^\pm$, $\pi_1^\pm$ and $\pi_8^\pm$, respectively, and therefore the total sum is finite.

By analytical evaluations of the Feynman diagrams, we find the effective $d\bar{s}Z$ vertex induced by the charged top-pion exchange,

$$\Gamma_{Z_\mu}^{I} = \frac{1}{16\pi^2}\frac{g^3}{\cos\theta_W}\sum_j \lambda_j \overline{s_L}\gamma_\mu d_L C_0(\xi_j), \quad (33)$$

with

$$C_0(\xi_j) = \frac{a_L^{ts*}a_L^{td}m_{\tilde{\pi}}^2}{2\sqrt{2}f_{\tilde{\pi}}^2 G_F M_W^2}\cdot T1(\xi_j), \quad (34)$$

$$T1(\xi_j) = \left[\frac{\xi_j(-1-3\xi_j+2\sin^2\theta_W(1+\xi_j))}{8(1-\xi_j)} - \frac{\xi_j^2\cos^2\theta_W}{2(1-\xi_j)^2}\ln\xi_j\right], \quad (35)$$

where $\lambda_j = V_{js}^* V_{jd}$, $\xi_t = m_t^{*2}/m_{\tilde{\pi}}^2$ with $m_t^* = (1-\epsilon)m_t$, $\xi_j = m_j^2/m_{\tilde{\pi}}^2$ for $j = c, u$.

For the case of unit-charged b-pion $\tilde{H}^\pm$, we have

$$\Gamma_{Z_\mu}^{II} = \frac{1}{16\pi^2}\frac{g^3}{\cos\theta_W}\sum_j \lambda_j \overline{s_R}\gamma_\mu d_R C_0(\eta_j), \quad (36)$$

with

$$C_0(\eta_j) = \frac{a_R^{ts*}a_R^{td}m_{\tilde{H}}^2}{2\sqrt{2}f_{\tilde{\pi}}^2 G_F M_W^2} \times \left[\frac{\eta_j(-1+\eta_j+2\sin^2\theta_W(1+\eta_j))}{8(1-\eta_j)} + \frac{\eta_j^2\sin^2\theta_W}{2(1-\eta_j)^2}\ln[\eta_j]\right], \quad (37)$$

where $\eta_t = m_t^{*2}/m_{\tilde{H}}^2$, $\eta_j = m_j^2/m_{\tilde{H}}^2$ for $j = c, u$.

For the case of technipions $\pi_1^\pm$ and $\pi_8^\pm$, we have

$$\Gamma_{Z_\mu}^{III} = \frac{1}{16\pi^2}\frac{g^3}{\cos\theta_W}\sum_j \lambda_j \overline{s_L}\gamma_\mu d_L C_0(y_j), \quad (38)$$

$$\Gamma_{Z_\mu}^{IV} = \frac{1}{16\pi^2}\frac{g^3}{\cos\theta_W}\sum_j \lambda_j \overline{s_L}\gamma_\mu d_L C_0(z_j), \quad (39)$$

with

$$C_0(y_j) = \frac{m_{\pi_1}^2}{3\sqrt{2}F_\pi^2 G_F M_W^2}\cdot T1(y_j), \quad (40)$$

$$C_0(z_j) = \frac{8m_{\pi_8}^2}{3\sqrt{2}F_\pi^2 G_{\rm F} M_{\rm W}^2} \cdot {\rm T1}(z_j), \tag{41}$$

where $y_{\rm t} = m_{\rm t1}^2/m_{\pi_1}^2$ and $z_{\rm t} = m_{\rm t1}^2/m_{\pi_8}^2$ with $m_{\rm t1} = \epsilon m_{\rm t}$, and $y_j = m_j^2/m_{\pi_1}^2$ and $z_j = m_j^2/m_{\pi_8}^2$ for $j = {\rm u, c}$.

The new C_0 functions in (34), (37), (40), and (41) are just the same kind of functions as the $\Gamma_{\rm Z}$ in (2.7) of [28] or the $C_0(x_i)$ in (2.18) of the first paper in [1]. Each new C_0 function describes the contribution to the $\bar{\rm d}$sZ vertex from the corresponding scalar. In the numerical calculations we will include the new contributions to the rare K decays by simply adding the new C_0 functions with their standard-model counterpart $C_0(x_i)$.

In the above calculations, we used the unitary relation $\sum_{j={\rm u,c,t}} \lambda_j \cdot {\rm const.} = 0$ wherever possible, and neglected the masses for all external quark lines. We also used the functions $(B_0, B_\mu, C_0, C_\mu, C_{\mu\nu})$ whenever needed to make the integrations, and the explicit forms of these complicated functions can be found, for instance, in Appendix A of [29].

When the new contributions from charged scalars are included, the functions $X(x_{\rm t})$, $Y(x_{\rm t})$, $P_0(X)$, and $P_0(Y)$ appearing in (28), (29), and (30) should be modified as follows:

$$X_{\rm tot} = X(x_{\rm t}) + X^{\rm New}, \tag{42}$$
$$Y_{\rm tot} = Y(x_{\rm t}) + X^{\rm New}, \tag{43}$$
$$P_0(X)_{\rm tot} = P_0(X) + P_0^{\rm New}, \tag{44}$$
$$P_0(Y)_{\rm tot} = P_0(Y) + P_0^{\rm New}, \tag{45}$$

with

$$X^{\rm New} = C_0(\xi_{\rm t}) + C_0(\eta_{\rm t}) + C_0(y_{\rm t}) + C_0(z_{\rm t}), \tag{46}$$
$$P_0^{\rm New} = \frac{1}{\lambda^4}\Big[C_{\rm NL}(\tilde{\pi}^\pm) + C_{\rm NL}(\tilde{\rm H}^\pm) + C_{\rm NL}(\pi_1^\pm) + C_{\rm NL}(\pi_8^\pm)\Big], \tag{47}$$

where the function $X^{\rm New}$ describes the correction from the dominant top-quark part, while the function $P_0^{\rm New}$ corresponds to the charm part. The new charm part is numerically very small: no more than 2% of the total new contribution. For the convenience of the reader, we present the explicit expressions of functions $C_{\rm NL}(\pi_i)$ ($\pi_i = \tilde{\pi}^\pm, \tilde{\rm H}^\pm, \pi_1^\pm, \pi_8^\pm$) in Appendix B.

In the SM, by using the SIP we have

$$X(x_{\rm t}) = 1.537, \quad Y(x_{\rm t}) = 1.032,$$
$$P_0(X) = 0.412, \quad P_0(Y) = 0.155. \tag{48}$$

For Case A, by using the SIP (20) and assuming $m_{\tilde{\pi}} = 100\,{\rm GeV}$ and $m_{\tilde{\rm H}} = 300\,{\rm GeV}$, we have

$$X(\xi_{\rm t}) = 2.258, \quad P_0^{\rm New}(\tilde{\pi}^\pm) = -0.0146, \tag{49}$$
$$X(\eta_{\rm t}) = -7\times 10^{-4}, \quad |P_0^{\rm New}(\tilde{\rm H}^\pm)| \le 10^{-6}. \tag{50}$$

Here it is easy to see that $X(\eta_{\rm t})$ and $P_0^{\rm New}(\tilde{\rm H}^\pm)$ are clearly much smaller than $X(\xi_{\rm t})$ and $P_0^{\rm New}(\tilde{\pi}^\pm)$. We therefore neglect the contribution from the b-pions $\tilde{\rm H}^\pm$ in Case A.

For Case B, by using the SIP (20) and assuming $m_{\tilde{\pi}} = 100\,{\rm GeV}$ and $m_{\tilde{\rm H}} = 300\,{\rm GeV}$, we have

$$X(\xi_{\rm t}) = 2.258, \quad P_0^{\rm New}(\tilde{\pi}^\pm) = -0.0146, \tag{51}$$
$$X(\eta_{\rm t}) = \pm 1.746, \quad P_0^{\rm New}(\tilde{\rm H}^\pm) = \pm 0.146, \tag{52}$$

where the sign of $X(\eta_{\rm t})$ and $P_0^{\rm New}(\tilde{\rm H}^\pm)$ will be determined by the sign of $a_{\rm R}^{\rm ts*}a_{\rm R}^{\rm td}$. Both $X(\eta_{\rm t})$ and $P_0^{\rm New}(\tilde{\rm H}^\pm)$ will be positive (negative) when the product $a_{\rm R}^{\rm ts*}a_{\rm R}^{\rm td}$ is negative (positive). In the following, we use the term Case B1 and Case B2 to denote the case of assuming $a_{\rm R}^{\rm ts*}a_{\rm R}^{\rm td} = 1/4, -1/4$, respectively. For Case B1 (Case B2), the new contributions from $\tilde{\pi}^\pm$ and $\tilde{\rm H}^\pm$ will cancel (enhance) each other.

In TC2 models, the new contribution to the rare K decays from ordinary technipions is strongly suppressed by a factor of $(\epsilon f_{\tilde{\pi}}/F_\pi)^2 \sim 10^{-3}$ for $F_\pi \approx 123\,{\rm GeV}$ and $\epsilon \approx 0.05$, when compared with that from the top-pions. Numerically, less than 5% of the total new contribution is due to $\pi_1^\pm$ and $\pi_8^\pm$. We therefore use the fixed values of $m_{\pi_1} = 50\,{\rm GeV}$ and $m_{\pi_8} = 100\,{\rm GeV}$ in the following numerical calculations. For heavier technipions, their contributions will become even smaller.

In the multiscale walking technicolor model [4], on the contrary, the enhancements to the rare K decays due to $\pi_1^\pm$ and $\pi_8^\pm$ can be as large as $2 \sim 3$ orders of magnitude. The major reason is the big difference in how to generate a large top-quark mass in different models, which in turn result in very different effective Yukawa couplings. In the TC2 models, $\pi_1^\pm$ and $\pi_8^\pm$ couple to the top quark with strength $\epsilon m_{\rm t}/F_\pi \approx 0.1$, which is much smaller than the coupling in the MWTCM: $m_{\rm t}/F_{\rm Q} \approx 4$ for $F_{\rm Q} \approx 40\,{\rm GeV}$ [4]. And finally the technipions $\pi_1^\pm$ and $\pi_8^\pm$ contribute to the rare K decays very differently in the MWTCM and the TC2 models.

Figure 2a and Fig. 2b show the X functions for Case A and Case B, respectively. The short-dashed line is the standard-model prediction $X(x_{\rm t}) = 1.537$. In Fig. 2a, the long-dashed curve shows the function $X(\xi_{\rm t})$ and the solid curve corresponds to the function $X_{\rm tot}$. The positive $X(\xi_{\rm t})$ greatly enhances the $X(x_{\rm t})$ for light $\tilde{\pi}^\pm$. In Fig. 2b, the dotted and solid curve show the function $X_{\rm tot}$ for Case B1 and Case B2, respectively.

Within the range of $\epsilon = 0.03 \sim 0.1$, the X functions basically remain unchanged. For $f_{\tilde{\pi}} = 60\,{\rm GeV}$, the functions $X(\xi_{\rm t})$ and $X(\eta_{\rm t})$ will be decreased by a factor of $(5/6)^2$.

In the following two sections we will present the numerical results for the branching ratios $B({\rm K}^+ \to \pi^+\nu\bar{\nu})$, $B({\rm K_L} \to \pi^0\nu\bar{\nu})$ and $B({\rm K_L} \to \mu^+\mu^-)_{\rm SD}$ with the inclusion of new physics effects and compare the theoretical predictions with the data that are currently available.

4 Rare decays $\mathbf{K^+ \to \pi^+\nu\bar{\nu}}$ and $\mathbf{K_L \to \pi^0\nu\bar{\nu}}$

4.1 The decay $\mathbf{K^+ \to \pi^+\nu\bar{\nu}}$

The rare decay ${\rm K}^+ \to \pi^+\nu\bar{\nu}$ is theoretically very clean and the long-distance contributions were known to be negligi-

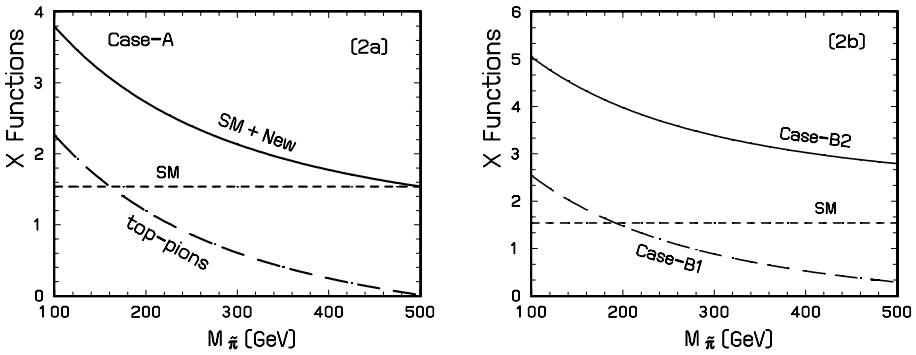

Fig. 2. Plots of the X functions versus the mass $m_{\tilde{\pi}}$ in the TC2-I model. See the text for more details

ble [1]. When the new contributions from scalars are included, one finds

$$B(\mathrm{K}^+ \to \pi^+ \nu\bar{\nu}) = \kappa_+ \cdot \left[\left(\frac{\mathrm{Im}\lambda_\mathrm{t}}{\lambda^5} X_\mathrm{tot} \right)^2 + \left(\frac{\mathrm{Re}\lambda_\mathrm{c}}{\lambda} P_0(X)_\mathrm{tot} + \frac{\mathrm{Re}\lambda_\mathrm{t}}{\lambda^5} X_\mathrm{tot} \right)^2 \right], \quad (53)$$

where $\kappa_+ = 4.11 \times 10^{-11}$ [1], the functions X_tot and $P_0(X)_\mathrm{tot}$ are given in (42) and (44).

Using the SIP (20), and assuming $m_{\tilde{\pi}} = (100\text{–}500)\,\mathrm{GeV}$ and $m_{\tilde{\mathrm{H}}} = 300\,\mathrm{GeV}$, we have

$$B(\mathrm{K}^+ \to \pi^+ \nu\bar{\nu}) = \begin{cases} 9.39 \times 10^{-11} & \text{in SM,} \\ (3.92\text{–}0.89) \times 10^{-10} & \text{in Case A,} \\ (1.95\text{–}0.13) \times 10^{-10} & \text{in Case B1,} \\ (6.59\text{–}2.34) \times 10^{-10} & \text{in Case B2.} \end{cases} \quad (54)$$

On the experimental side, the first event for $\mathrm{K}^+ \to \pi^+ \nu\bar{\nu}$ has been recently observed by the BNL787 collaboration [6], giving

$$B(\mathrm{K}^+ \to \pi^+ \nu\bar{\nu})_\mathrm{exp} = 4.2^{+9.7}_{-3.5} \times 10^{-10}, \quad (55)$$

in the ball park of the SM expectations. Further data already collected are expected to increase the sensitivity by more than a factor of 2, and there are plans to collect data representing a further large increase in sensitivity.

Figure 3a and Fig. 3b show the $m_{\tilde{\pi}}$ dependence of $B(\mathrm{K}^+ \to \pi^+ \nu\bar{\nu})$ in Case A and Case B, respectively. In Fig. 3, the horizontal band between two solid lines corresponds to the data (55), while the short-dashed line is the standard-model prediction. The solid curve in Fig. 3a shows the branching ratio $B(\mathrm{K}^+ \to \pi^+ \nu\bar{\nu})$ when the new contributions are included. In Fig. 3b, the lower (upper) solid and short-dashed curve are the branching ratios $B(\mathrm{K}^+ \to \pi^+ \nu\bar{\nu})$ in Case B1 (Case B2) for $m_{\tilde{\mathrm{H}}} = 300$ and 1000 GeV, respectively.

From Fig. 3b, an upper bound on $m_{\tilde{\pi}}$ can be read out: $m_{\tilde{\pi}} \le 285\,\mathrm{GeV}$ for $m_{\tilde{\mathrm{H}}} \le 1000\,\mathrm{GeV}$ in Case B1. This upper bound will be weakened by about 50 GeV if we consider uncertainties of other parameters.

From Fig. 3 one can see that the theoretical predictions for the branching ratio $B(\mathrm{K}^+ \to \pi^+ \nu\bar{\nu})$ in the TC2-I model are now in good agreement with the data (55) for all three cases. The uncertainty of the data is still large. Further improvement of the data will be very helpful to constrain the TC2 models from this decay mode.

4.2 The decay $\mathbf{K_L \to \pi^0 \nu\bar{\nu}}$

In the SM, the rare decay $\mathrm{K_L} \to \pi^0 \nu\bar{\nu}$ is completely dominated by short-distance loop effects with the top-quark exchanges, and there are no theoretical uncertainties due to $m_\mathrm{c}, \mu_\mathrm{c}$ and $\Lambda_{\overline{\mathrm{MS}}}$ present in the decay $\mathrm{K}^+ \to \pi^+ \nu\bar{\nu}$. Consequently this decay mode is even cleaner than $\mathrm{K}^+ \to \pi^+ \nu\bar{\nu}$ and is very well suited for the probe of new physics if the experimental data can reach the required sensitivity.

When the new contributions from scalars are included, the branching ratio will be

$$B(\mathrm{K_L} \to \pi^0 \nu\bar{\nu}) = \kappa_\mathrm{L} \cdot \left(\frac{\mathrm{Im}\lambda_\mathrm{t}}{\lambda^5} X_\mathrm{tot} \right)^2. \quad (56)$$

where $\kappa_\mathrm{L} = 1.80 \times 10^{-10}$ [1]; the function X_tot is given in (42).

Using the SIP (20) and assuming $m_{\tilde{\pi}} = (100\text{–}500)\,\mathrm{GeV}$ and $m_{\tilde{\mathrm{H}}} = 300\,\mathrm{GeV}$, we have

$$B(\mathrm{K_L} \to \pi^0 \nu\bar{\nu}) = \begin{cases} 2.74 \times 10^{-11} & \text{in SM,} \\ (1.67\text{–}0.28) \times 10^{-10} & \text{for Case A,} \\ (0.75\text{–}0.01) \times 10^{-10} & \text{for Case B1,} \\ (2.95\text{–}0.91) \times 10^{-10} & \text{for Case B2.} \end{cases} \quad (57)$$

On the experimental side, the KTeV group has recently quoted a preliminary result [30]

$$B(\mathrm{K_L} \to \pi^0 \nu\bar{\nu}) \le 1.8 \times 10^{-6}, \quad 90\%\ \mathrm{CL}, \quad (58)$$

and the same group aims at reaching a single event sensitivity of 3×10^{-9} in 1999 [31]. The CLOE experiment in DAΦNE can also reach a sensitivity of 10^{-9} in the next few years [32]

Figure 4 shows the $m_{\tilde{\pi}}$ dependence of $B(\mathrm{K_L} \to \pi^0 \nu\bar{\nu})$ in all three cases. The short-dashed line is the standard-model prediction. The middle solid curve is the branching ratio in Case A, while the lower (upper) two curves are the branching ratios in Case B1 (Case B2) for $m_{\tilde{\mathrm{H}}} = 300$

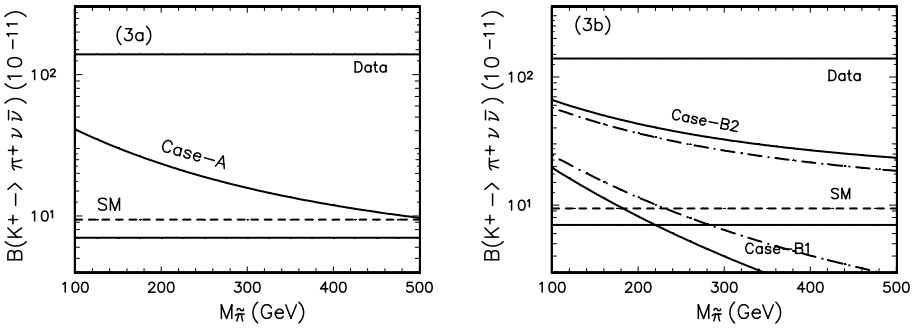

Fig. 3. The branching ratio $B(K^+ \to \pi^+\nu\bar{\nu})$ in the TC2-I model as a function of $m_{\tilde{\pi}}$ for Case A and Case B. The short-dashed line is the SM prediction, while the horizontal band shows the data (55). The solid curve in **a** is the branching ratio in Case A, while the lower (upper) two curves in **b** show the ratios in Case B1 (Case B2) for $m_{\tilde{H}} = 300$ and 1000 GeV, respectively

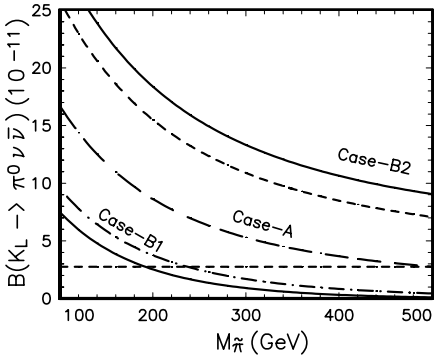

Fig. 4. The branching ratio $B(K_L \to \pi^0\nu\bar{\nu})$ in the TC2-I model as functions of $m_{\tilde{\pi}}$. The short-dashed line is the SM prediction. The long-dashed curve is the ratio in Case A, while the lower (upper) two curves show the ratios in Case B1 (Case B2) for $m_{\tilde{H}} = 300$ and 1000 GeV, respectively

and 1000 GeV, respectively. The enhancement can be as large as one order of magnitude for Case B2.

Although the current bound (58) is still about four orders of magnitude above the theoretical expectation after including the contributions from new scalars, it is possible to measure this gold-plated decay mode with enough sensitivity to probe the effects of new physics in next few years. Sensitivities around 10^{-11} are the goal of three dedicated experiments which have been recently proposed [31, 33,34]. A recent proposal [33], for example, aims to make a ∼15% measurement of $B(K_L \to \pi^0\nu\bar{\nu})$.

5 The decay $K_L \to \mu^+\mu^-$

The rare decay $K_L \to \mu^+\mu^-$ is a potentially important channel to study the weak interaction within the SM, as well as possible effects of new physics. This decay proceeds through two different mechanisms: a dominant long-distance (LD) part from the two-photon intermediate state and a short-distance (SD) part, which in the SM arises from one-loop Z^0 penguin and W box diagrams involving gauge bosons. Since the short-distance part is sensitive to the presence of a virtual top quark and other new heavy particles predicted by many new physics models[2], it offers a window into new physics phenomena.

[2] In TC2 models, for example, the virtual unit-charged scalars will appear in the Z^0 penguin diagrams as shown in Fig. 1, and thus provide new contributions to the rare K decays.

For the decay $K_L \to \mu^+\mu^-$, the full branching ratio can be written generally as follows [35]:

$$B(K_L \to \mu^+\mu^-) = 2\beta B(K_L \to \gamma\gamma)\left(\frac{\alpha m_\mu}{\pi M_K}\right)^2 \times \left(\mathrm{Re}[A]^2 + \mathrm{Im}[A]^2\right), \quad (59)$$

$$\mathrm{Re}[A] = A_{SD} + A_{LD}, \quad (60)$$

where $\beta = \sqrt{1 - 4m_\mu^2/M_K^2}$, $\mathrm{Im}[A]$ denote the absorptive contribution arising from a two-photon intermediate state, and finally A_{SD} and A_{LD} represent the short- and long-distance dispersive contribution, respectively.

In the SM, the short-distance part of $B(K_L \to \mu^+\mu^-)$ is [1]

$$B(K_L \to \mu^+\mu^-)_{SD} = (1.23 \pm 0.57) \times 10^{-9}, \quad (61)$$

where the error is dominated by the uncertainty of $|V_{cb}|$. Using the measured branching ratio of $B(K_L \to \gamma\gamma) = (5.92 \pm 0.12) \times 10^{-4}$ [25], one gets

$$B(K_L \to \mu^+\mu^-)_{abs} = (7.07 \pm 0.18) \times 10^{-9}, \quad (62)$$

which is very close to the measured rate [7,25]

$$B(K_L \to \mu^+\mu^-) = (7.2 \pm 0.5) \times 10^{-9}. \quad (63)$$

It is easy to see that the rate $B(K_L \to \mu^+\mu^-)$ is almost saturated by the absorptive contribution, leaving only small room for the coherent sum of the long- and short-distance dispersive contribution,

$$B(K_L \to \mu^+\mu^-)_{dis}^{(LD+SD)} = (0.1 \pm 0.5) \times 10^{-9}. \quad (64)$$

Therefore, the magnitude of the total real part $\mathrm{Re}[A]$ must be relatively small compared with the absorptive part[3]. Such a small total dispersive amplitude can be realized either when the A_{SD} and A_{LD} parts are both small or by partial cancellation between these two parts.

In [35], the authors estimated the dispersive two-photon contribution to the decays $P \to l^+l^-$ ($P = \pi^0$,

[3] The data constrains only the size of $\mathrm{Re}[A]$, and thus leaves an ambiguity for the sign of $\mathrm{Re}[A]$.

η, K_L, and $l = e, \mu$) in the framework of the chiral perturbation theory and large-N_C considerations and found that

$$\begin{aligned}\mathrm{Re}[A(P\to l^+l^-)] &= \frac{1}{4\beta}\ln^2\left[\frac{1-\beta}{1+\beta}\right]+\frac{1}{\beta}Li_2\left[\frac{\beta-1}{\beta+1}\right]\\ &\quad+\frac{\pi^2}{12\beta}+3\ln\left[\frac{m_l}{M_\rho}\right]+\chi(M_\rho) \qquad (65)\\ &= \begin{cases} 3.2^{+0.8}_{-1.0}, & \text{for } \eta\to\mu^+\mu^-,\\ 2.9^{+0.8}_{-1.0}-A_{\mathrm{SD}}, & \text{for } K_L\to\mu^+\mu^-,\end{cases}\end{aligned}$$

where $M_\rho = 0.77\,\mathrm{GeV}$ is the mass of ρ meson, and $\chi(M_\rho) = 5.5^{+0.8}_{-1.0}$ is the local contribution determined by fitting the measured ratio $B(\eta\to\mu^+\mu^-) = (5.8\pm0.8)\times10^{-6}$ [25]. The relative sign between the short- and long-distance dispersive amplitude in (66) is fixed by the known positive sign of g_8 in the large-N_c limit [36]. From the measured branching ratios of $\eta\to\mu^+\mu^-$ and $K_L\to\mu^+\mu^-$ decays, constraints on the short-distance part A_{SD} of the decay $K_L\to\mu^+\mu^-$ were derived [35]:

$$A_{\mathrm{SD}} = \begin{cases} 2.2^{+1.1}_{-1.3}, & \text{for } \mathrm{Re}[A]>0,\\ 3.6\pm1.2, & \text{for } \mathrm{Re}[A]<0.\end{cases} \qquad (66)$$

The first bound is in good agreement with the standard-model expectation $A_{\mathrm{SD}}^{\mathrm{SM}} = 1.8\pm0.6$ [35], while the second bound shows a discrepancy of about 1.4σ with the SM expectation. However, the errors of above two bounds could be reduced by improving the measurements of the branching ratio $\eta\to\mu^+\mu^-$ and $K_L\to\mu^+\mu^-$. From (66) and (66), one can see that the short- and long-distance dispersive contributions are comparable in size but cancel each other strongly. The above bounds on A_{SD} can be translated into the constraints on $B(K_L\to\mu^+\mu^-)_{\mathrm{SD}}$ directly,

$$B(K_L\to\mu^+\mu^-)_{\mathrm{SD}} = \qquad (67)$$
$$\begin{cases} (0.2\text{–}2.8)\times10^{-9}, & (\text{Bound 1}: \text{ for } \mathrm{Re}[A]>0),\\ (1.5\text{–}6.0)\times10^{-9}, & (\text{Bound 2}: \text{ for } \mathrm{Re}[A]<0).\end{cases}$$

Obviously, the bounds are still relatively weak because of the sign ambiguity of $\mathrm{Re}[A]$.

In the SM, the branching ratio $B(K_L\to\mu^+\mu^-)_{\mathrm{SD}}$ is known at the NLO level [1], as given in (61). By comparing the above bounds on $B(K_L\to\mu^+\mu^-)_{\mathrm{SD}}$ with the theoretical predictions after including new physics contributions, one may find useful information on TC2 models.

When the new contributions from scalars in TC2-I model are included, we have

$$\begin{aligned}B(K_L\to\mu^+\mu^-)_{\mathrm{SD}} = \kappa_\mu\cdot\Bigg[&\frac{\mathrm{Re}\lambda_c}{\lambda}P_0(Y)_{\mathrm{tot}}\\ &+\frac{\mathrm{Re}\lambda_t}{\lambda^5}Y_{\mathrm{tot}}\Bigg]^2. \qquad (68)\end{aligned}$$

where $\kappa_\mu = 1.68\times10^{-9}$ [1], the functions Y_{tot} and $P_0(Y)_{\mathrm{tot}}$ are given in (43) and (45). Using the SIP (20) and assuming $m_{\tilde\pi} = (100\text{–}500)\,\mathrm{GeV}$ and $m_{\tilde H} = 600\,\mathrm{GeV}$, one gets

$$B(K_L\to\mu^+\mu^-)_{\mathrm{SD}} = \qquad (69)$$
$$\begin{cases} 1.25\times10^{-9} & \text{in SM},\\ (9.18\text{–}1.13)\times10^{-9} & \text{for Case A},\\ (4.57\text{–}0.03)\times10^{-9} & \text{for Case B1},\\ (15.36\text{–}3.81)\times10^{-9} & \text{for Case B2}.\end{cases}$$

The enhancement can reach one order of magnitude.

Figure 5a shows the branching ratio $B(K_L\to\mu^+\mu^-)_{\mathrm{SD}}$ versus the mass $m_{\tilde\pi}$ for Case A and Case B1. The short-dashed line is the SM prediction, while the horizontal band here corresponds to Bound 1. The upper solid curve in Fig. 5a shows the branching ratio $B(K_L\to\mu^+\mu^-)_{\mathrm{SD}}$ in Case A, and a lower bound $m_{\tilde\pi}\geq 280\,\mathrm{GeV}$ can be read out. The lower three curves in Fig. 5a are the ratios $B(K_L\to\mu^+\mu^-)_{\mathrm{SD}}$ in Case B1 for $m_{\tilde H} = 300, 600$ and $1000\,\mathrm{GeV}$, respectively.

Figure 5b shows the same as Fig. 5a, but the horizontal band here stands for Bound 2. For Case A, the theoretical prediction is consistent with the bound, while Bound 2 prefers light top-pions for Case B1: $m_{\tilde\pi}\leq 230\,\mathrm{GeV}$ for $m_{\tilde H}\leq 1000\,\mathrm{GeV}$.

Figure 6a and Fig. 6b show the same as Fig. 5a and Fig. 5b but for Case B2 instead. The upper three curves in Figs. 6a and 6b are the ratios $B(K_L\to\mu^+\mu^-)_{\mathrm{SD}}$ in Case B2 for $m_{\tilde H} = 300, 600$ and $1000\,\mathrm{GeV}$, respectively. Case B2 is completely excluded if $\mathrm{Re}[A]>0$, but is still allowed if $\mathrm{Re}[A]<0$ and $m_{\tilde\pi}\geq 270\,\mathrm{GeV}$.

For the decay $K_L\to\mu^+\mu^-$, there is a strong cancellation between the short- and long-distance dispersive parts. For Case A, the enhancement to $B(K_L\to\mu^+\mu^-)_{\mathrm{SD}}$ can reach a factor of 8 for light top-pions. For Case B1 (Case B2), the new contributions from top-pions and b-pions will cancel (enhance) each other, and the resultant enhancement can reach a factor of 4 (12) for light top-pions.

6 Conclusion and discussions

In this paper we calculated the new contributions to the rare FCNC K decays $K^+\to\pi^+\nu\bar\nu$, $K_L\to\pi^0\nu\bar\nu$ and $K_L\to\mu^+\mu^-$ from the new Z^0 penguin and box diagrams induced by the unit-charged top-pions $\tilde\pi^\pm$, b-pions $\tilde H^\pm$, and technipions $\pi_1^\pm$ and $\pi_8^\pm$ appearing in the TC2 models. We choose the TC2-I model proposed by Hill [8] as the typical TC2 model to do the analytical and numerical calculations. It is beyond the scope of this paper to consider the detailed differences between TC2 models.

From the analytical evaluations of the one-loop Feynman diagrams, we extract the new functions $C_0(\pi_i)$ and $C_{\mathrm{NL}}(\pi_i)$ ($\pi_i = \tilde\pi^\pm, \tilde H^\pm, \pi_1^\pm, \pi_8^\pm$) which describe the new Z^0 penguin contributions due to unit-charged scalars, combine the new functions with their standard-model counterparts and use them directly in the calculation of branching ratios. The m_t-dependent term X^{New} in (46) dominates over the m_t-independent term P_0^{New} in (47).

The mixing matrixes D_L and D_R also play an important role for the characteristics and magnitudes of the new

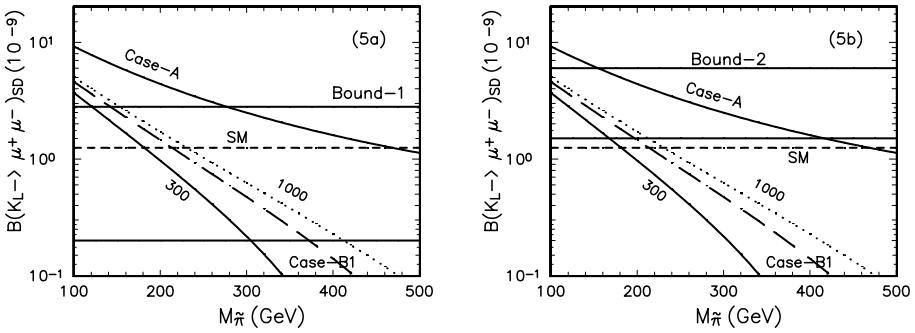

Fig. 5. The branching ratio $B(\mathrm{K_L} \to \mu^+\mu^-)_{\rm SD}$ as a function of $m_{\tilde{\pi}}$ for Case A and Case B1. The short-dashed line is the SM prediction. The horizontal band in **a** (**b**) corresponds to Bound 1 (Bound 2). The upper solid curve stands for the ratio in Case A, while the lower three curves show the ratios in Case B1 for $m_{\tilde{\rm H}} = 300, 600$ and 1000 GeV, respectively

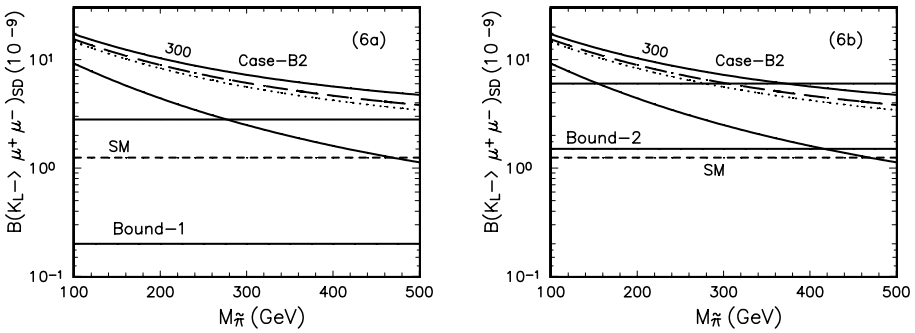

Fig. 6. The same as in Fig. 5, but for Case B2

contributions, but unfortunately these new mixing matrices are really the most undetermined part of the TC2 models. Thanks to the accurate experimental measurement of $\mathrm{B^0}$–$\overline{\mathrm{B^0}}$ mixing, we got some strong constraints (16) and (19) on the relevant mixing factors. Case A is allowed by the constraints (16) and (19), while Case B1 and Case B2 are also considered for the purpose of comparison and illustration.

For the decay $\mathrm{K^+} \to \pi^+\nu\overline{\nu}$, the enhancement to the ratio $B(\mathrm{K^+} \to \pi^+\nu\overline{\nu})$ can reach a factor of $2 \sim 7$. The theoretical predictions in the TC2-I model generally agree well with the data (55) for all three cases. Of course, the uncertainty of the data is still very large and further improvement of the data will be very helpful to test or constrain the TC2 models from this decay mode.

The decay $\mathrm{K_L} \to \pi^0\nu\overline{\nu}$ is the cleanest decay mode among the three decay modes in question. The enhancement to the branching ratio $B(\mathrm{K_L} \to \pi^0\nu\bar{\nu})$ due to the top-pions and b-pion can be as large as one order of magnitude. But the central problem for this decay mode is the very low sensitivity of the available data, which is about four orders of magnitude above the theoretical expectation. Further improvements of the data will be very essential to find the signals of new physics through this decay mode.

For the decay $\mathrm{K_L} \to \mu^+\mu^-$, the situation becomes more complicated because of the involvement of the long-distance contributions. After including the additional short-distance part from new physics, the theoretical predictions are still consistent with the data for Case A and Case B1. Case B2, however, is disfavored by the data. The major obstacles in extracting strong constraints on $A_{\rm SD}$ out of the decay $\mathrm{K_L} \to \mu^+\mu^-$ is the large uncertainty of $A_{\rm LD}$, the sign ambiguity of $\mathrm{Re}[A]$ as well as the strong cancellation between the short- and long-distance dispersive parts. Therefore improvements in theoretical predictions and the experimental data will be very essential for us to test the new physics effects through this decay mode.

In summary, the unit-charged scalars appearing in TC2 models can provide sizable new contributions to the rare K decays $\mathrm{K^+} \to \pi^+\nu\overline{\nu}$, $\mathrm{K_L} \to \pi^0\nu\overline{\nu}$ and $\mathrm{K_L} \to \mu^+\mu^-$ through $\mathrm{Z^0}$ penguin diagrams. The accurate data of $\mathrm{B^0}$–$\overline{\mathrm{B^0}}$ mixing lead to strong constraints on the size of $D_{\rm R}^{\rm bd}$ and $D_{\rm R}^{\rm bs}$ if we use the square-root ansatz for the $D_{\rm L}$. Some simple but interesting lower or upper bounds on $m_{\tilde{\pi}}$ are obtained by comparing the theoretical predictions with the relevant data. The TC2-I model is, in general, still consistent with the available data of the rare K decays in question. Further improvement of the data and the theoretical predictions will be very helpful to constrain the TC2 models from the rare K decays.

Acknowledgements. This work is supported in part by the National Natural Science Foundation of China under Grant No. 19575015, and by the Outstanding Young Teacher Foundation of the Education Ministry of China, as well as by the funds from Henan Science and Technology Committee.

Appendix A

In this Appendix, we present the explicit expressions for the functions $B_0(x_{\rm t})$, $C_0(x_{\rm t})$, $X_1(x_{\rm t})$, and $Y_1(x_{\rm t})$. The functions of $C_0(x_{\rm t})$ and $B_0(x_{\rm t})$ govern the leading top-quark contributions through the $\mathrm{Z^0}$ penguin and W box diagrams in the SM, while the functions $X_1(x_{\rm t})$ and $Y_1(x_{\rm t})$ describe the NLO QCD corrections:

$$B_0(x_{\rm t}) = \frac{1}{4}\left[\frac{x_{\rm t}}{1-x_{\rm t}} + \frac{x_{\rm t}\ln[x_{\rm t}]}{(x_{\rm t}-1)^2}\right], \qquad \text{(A1)}$$

$$C_0(x_t) = \frac{x_t}{8}\left[\frac{x_t-6}{x_t-1} + \frac{3x_t+2}{(x_t-1)^2}\ln[x_t]\right], \quad \text{(A2)}$$

$$X_1(x_t) = -\frac{23x_t+5x_t^2-4x_t^3}{3(1-x_t)^2} + \frac{x_t-11x_t^2+x_t^3+x_t^4}{(1-x_t)^3}\ln[x_t] + \frac{8x_t+4x_t^2+x_t^3-x_t^4}{2(1-x_t)^3}\ln^2[x_t] - \frac{4x_t-x_t^3}{(1-x_t)^2}L_2(1-x_t) + 8x_t\frac{\partial X_0(x_t)}{\partial x_t}\ln[x_\mu], \quad \text{(A3)}$$

$$Y_1(x_t) = -\frac{4x_t+16x_t^2+4x_t^3}{3(1-x_t)^2} - \frac{4x_t-10x_t^2-x_t^3-x_t^4}{(1-x_t)^3}\ln[x_t] + \frac{2x_t-4x_t^2+x_t^3-x_t^4}{2(1-x_t)^3}\ln^2[x_t] - \frac{2x_t+x_t^3}{(1-x_t)^2}L_2(1-x_t) + 8x_t\frac{\partial Y_0(x_t)}{\partial x_t}\ln[x_\mu], \quad \text{(A4)}$$

where $x_t = m_t^2/m_W^2$, $x_\mu = \mu^2/M_W^2$ with $\mu = \mathcal{O}(m_t)$ and

$$L_2(1-x_t) = \int_1^{x_t} dy \frac{\ln[y]}{1-y}. \quad \text{(A5)}$$

For the charm sector in the SM, the C_{NL} is the Z^0 penguin part and the $B_{NL}^{1/2}$ ($B_{NL}^{-1/2}$) is the box contribution, relevant for the case of final state leptons with $T_3 = 1/2$ ($T_3 = -1/2$):

$$C_{NL} = \frac{x(m)}{32}K_c^{24/25}\left[\left(\frac{48}{7}K_+ + \frac{24}{11}K_- - \frac{696}{77}K_{k33}\right)\times\left(\frac{4\pi}{\alpha_s(\mu)} + \frac{15212}{1875}(1-K_c^{-1})\right) + \left(1-\ln\frac{\mu^2}{m^2}\right)(16K_+ - 8K_-) - \frac{1176244}{13125}K_+ - \frac{2302}{6875}K_- + \frac{3529184}{48125}K_{33} + K\left(\frac{56248}{4375}K_+ - \frac{81448}{6875}K_- + \frac{4563698}{144375}K_{33}\right)\right], \quad \text{(A6)}$$

where

$$K = \frac{\alpha_s(M_W)}{\alpha_s(\mu)}, \quad K_c = \frac{\alpha_s(\mu)}{\alpha_s(m)},$$
$$K_+ = K^{6/25}, \quad K_- = K^{-12/25}, \quad K_{33} = K^{-1/25} \quad \text{(A7)}$$

and

$$B_{NL}^{1/2} = \frac{x(m)}{4}K_c^{24/25}\left[3(1-K_2)\times\left(\frac{4\pi}{\alpha_s(\mu)} + \frac{15212}{1875}(1-K_c^{-1})\right) - \ln\frac{\mu^2}{m^2} - \frac{r\ln r}{1-r} - \frac{305}{12} + \frac{15212}{625}K_2 + \frac{15581}{7500}KK_2\right], \quad \text{(A8)}$$

$$B_{NL}^{-1/2} = \frac{x(m)}{4}K_c^{24/25}\left[3(1-K_2)\times\left(\frac{4\pi}{\alpha_s(\mu)} + \frac{15212}{1875}(1-K_c^{-1})\right) - \ln\frac{\mu^2}{m^2} - \frac{329}{12} + \frac{15212}{625}K_2 + \frac{30581}{7500}KK_2\right]. \quad \text{(A9)}$$

Here $K_2 = K_{33}$, $m = m_c$, $\mu = \mathcal{O}(m_c)$, $x(m) = m_c^2/M_W^2$, $r = m_l^2/m_c^2(\mu)$ and m_l is the lepton mass.

Appendix B

For the dominant top sector in the TC2-I model, the $C_0(\pi_i)$ ($\pi_i = \tilde{\pi}^\pm, \tilde{H}^\pm, \pi_1^\pm, \pi_8^\pm$) functions have been given in (34)–(37).

For the charm sector in the TC2-I model, the $C_{NL}(\pi_i)$ ($\pi_i = \tilde{\pi}^\pm, \tilde{H}^\pm, \pi_1^\pm, \pi_8^\pm$) functions take the form

$$C_{NL}(\pi_i) = a_i\frac{m_c^2}{m_W^2}K_c^{24/25}\left[\left(\frac{48}{7}K_+ + \frac{24}{11}K_- - \frac{696}{77}K_{33}\right)\times\left(\frac{4\pi}{\alpha_s(\mu)} + \frac{15212}{1875}(1-K_c^{-1})\right) + \left(1-\ln\frac{\mu^2}{m^2}\right)\times(16K_+ - 8K_-) - \frac{1176244}{13125}K_+ - \frac{2302}{6875}K_- + \frac{3529184}{48125}K_{33} + K_{\pi_i}\left(\frac{56248}{4375}K_+ - \frac{81448}{6875}K_- + \frac{4563698}{144375}K_{33}\right)\right], \quad \text{(B1)}$$

with

$$K_c = \frac{\alpha_s(\mu)}{\alpha_s(m_c)}, \quad K_{\pi_i} = \frac{\alpha_s(m_{\pi_i})}{\alpha_s(\mu)}, \quad K_+ = (K_{\pi_i})^{6/25},$$
$$K_- = (K_{\pi_i})^{-12/25}, \quad K_{33} = (K_{\pi_i})^{-1/25},$$
$$\mu = \mathcal{O}(m_c). \quad \text{(B2)}$$

For top-pion $\tilde{\pi}^\pm$ and b-pion $\tilde{H}^\pm$ we have

$$a_1 = \frac{a_L^{ts*}a_L^{td}}{64\sqrt{2}f_{\tilde{\pi}}^2G_F}, \quad K_{\tilde{\pi}} = \frac{\alpha_s(m_{\tilde{\pi}})}{\alpha_s(\mu)},$$
$$a_2 = \frac{a_R^{ts*}a_R^{td}}{8\sqrt{2}f_{\tilde{\pi}}^2G_F}, \quad K_{\tilde{H}} = \frac{\alpha_s(m_{\tilde{H}})}{\alpha_s(\mu)}. \quad \text{(B3)}$$

For ordinary technipions $\pi_1^\pm$ and $\pi_8^\pm$ we have

$$a_3 = \frac{1}{96\sqrt{2}F_\pi^2G_F}, \quad K_{\pi_1^\pm} = \frac{\alpha_s(m_{\pi_1})}{\alpha_s(\mu)},$$
$$a_4 = \frac{1}{12\sqrt{2}F_\pi^2G_F}, \quad K_{\pi_8^\pm} = \frac{\alpha_s(m_{\pi_8})}{\alpha_s(\mu)}. \quad \text{(B4)}$$

References

1. A.J. Buras, R. Fleischer, hep-ph/9704376, to appear in Heavy Flavor II, edited by A.J. Buras, M. Lindner (World Scientific, Singapore); G. Buchalla, A.J. Buras, M.E. Lautenbacher, Rev. Mod. Phys. **68**, 1125 (1996)

2. M. Misiak, S. Pokorski, J. Rosiek, hep-ph/9703442, to appear in Heavy Flavor II, edited by A.J. Buras, M. Lindner (World Scientific, Singapore)
3. A.J. Buras, A. Remanino, L. Silverstrini, Nucl. Phys. B **520**, 3 (1998); G. Valencia, Nucl. Phys. B **517**, 33 (1998); G.-C. Cho, Eur. Phys. J. C **5**, 525 (1998)
4. Z.J. Xiao, L.X. Lü, H.K. Guo, G.R. Lu, Eur. Phys. J. C**7**, 487 (1999)
5. C.D. Lü, Z.J. Xiao, Phys. Rev. D **53**, 2529 (1996); G.R. Lu, Z.H. Xiong, Y.G. Cao, Nucl. Phys. B **487**, 355 (1997); Z.J. Xiao et al., Commun. Theor. Phys. **29**, 431 (1998); Z.J. Xiao, L.X. Lü, H.K. Guo, G.R. Lu, Chin. Phys. Lett. **16**, 88 (1999)
6. S. Adler et al., Phys. Rev. Lett. **79**, 2204 (1997)
7. A.P. Heinson et al., Phys. Rev. D **51**, 985 (1995); T. Akagi et al., Phys. Rev. Lett. **67**, 2618 (1991); T. Akagi et al., KEK 137, Phys. Rev. D **51**, 2061 (1995)
8. C.T. Hill, Phys. Lett. **345B**, 483 (1995); K. Lane, E. Eichten, Phys. Lett. **352B**, 382 (1995)
9. S. Weinberg, Phys. Rev. D **13**, 974 (1976); **19**, 1277 (1979); L. Susskind, Phys. Rev. D **20**, 2619 (1979)
10. E. Farhi, L.Susskind, Phys. Rev. D **20**, 3404 (1979)
11. S. Dimopoulos, L. Susskind, Nucl. Phys. B **155**, 237 (1979); E. Eichten, K. Lane, Phys. Lett. **90B**, 125 (1980)
12. B. Holdom, Phys. Rev. D **24**, 1441 (1981); T. Appelquist, D. Karabali, L.C.R. Wijewardhana, Phys. Rev. Lett. **57**, 957 (1986)
13. M. Luty, R. Sundrum, Phys. Rev. Lett. **70**, 529 (1993); R. Sundrum, S. Hsu, Nucl. Phys. B **391**, 127 (1993); T. Appelquist, J. Terning, Phys. Lett. **315B**, 139 (1993)
14. K. Lane, E. Eichten, Phys.Lett. **222B**, 274 (1989); K. Lane, M.V. Ramana, Phys.Rev. D **44**, 2678 (1991)
15. K. Lane, presented at the 28th International Conference on High Energy Physics, Warsaw, July 1996, ICHEP 96:367-378; G. Burdman, hep-ph/9802232
16. K. Lane, Phys. Lett. B **433**, 96 (1998)
17. G. Burdman, D. Kominis, Phys. Lett. B **403**, 101 (1997); G. Burdman, Phys. Lett. B **409**, 443 (1997)
18. Y. Su, F. Bonini, D. Kominis, Phys. Rev. Lett. **79**, 4075 (1997)
19. G. Buchalla, G. Burdman, C.T. Hill, D. Kominis, Phys. Rev. D **53**, 5185 (1996)
20. G. Burdman, hep-ph/9611265
21. D. Kominis, Phys. Lett. B **358**, 312 (1995)
22. E. Eichten, I. Hinchliffe, K. Lane, C. Quigg, Rev. Mod. Phys. **56**, 759 (1984); Phys. Rev. D **34**, 1547 (1986); E. Eichten, K. Lane, Phys. Lett. **327B**, 129 (1994)
23. J. Ellis, M.K. Gaillard, D.V. Nanopoulos, P. Sikivie, Nucl. Phys. B **182**, 505 (1981)
24. K. Lane, Phys. Rev. D **54**, 2204 (1996)
25. Particle Data Group, C. Caso et al., Eur. Phys. J. C **3**, 1 (1998)
26. J.M. Flynn, plenary talk at the 28th International Conference on High Energy Physics, Warsaw, July 1996, and hep-lat/9611016
27. G. Buchalla, A.J. Buras, M.K. Harlander, Nucl. Phys. B **349**, 1 (1991)
28. T. Inami, C.S. Lim, Prog. Theor. Phys. **65**, 297 (1981)
29. P. Cho, B. Greistein, Nucl. Phys. B **365**, 365 (1991)
30. R. Ben-David, XVI International Workshop on Weak Interactions and Neutrinos, Capri, 1997
31. E. Chen et al., FERMILAB-PUB-97-321-E, hep-ex/9709026(1997)
32. F. Bossi, G. Colangelo, G. Isidori, Eur. Phys. J. C **6**, 109 (1999)
33. I.-H. Chiang et al., AGS Proposal 926 (1996)
34. T. Inagaki et al., KEK-96/13 (1996);
35. D. Gómez Dumm, A. Pich, Phys. Rev. Lett. **80**, 4633 (1998)
36. A. Pich, E. de Rafael, Phys. Lett. B **374**, 186 (1996)